



# Conformation of the Solute-Binding Protein AdcAll Influences Zinc Uptake in *Streptococcus pneumoniae*

Marina L. Župan<sup>1</sup>, Zhenyao Luo<sup>2,3,4</sup>, Katherine Ganio<sup>1</sup>, Victoria G. Pederick<sup>5</sup>,  
Stephanie L. Neville<sup>1</sup>, Evelyne Deplazes<sup>6,7</sup>, Boštjan Kobe<sup>2,3,4†</sup>  
and Christopher A. McDevitt<sup>1\*†</sup>

## OPEN ACCESS

### Edited by:

Guangchun Bai,  
Albany Medical College, United States

### Reviewed by:

Tiffany Zarrella,  
National Institutes of Health (NIH),  
United States  
Julia Martin,  
Idaho State University, United States

### \*Correspondence:

Christopher A. McDevitt  
christopher.mcdevitt@unimelb.edu.au

<sup>†</sup>These authors share last authorship

### Specialty section:

This article was submitted to  
Molecular Bacterial Pathogenesis,  
a section of the journal  
Frontiers in Cellular and  
Infection Microbiology

**Received:** 24 June 2021

**Accepted:** 27 July 2021

**Published:** 19 August 2021

### Citation:

Župan ML, Luo Z, Ganio K,  
Pederick VG, Neville SL, Deplazes E,  
Kobe B and McDevitt CA (2021)  
Conformation of the Solute-Binding  
Protein AdcAll Influences Zinc Uptake  
in *Streptococcus pneumoniae*.  
*Front. Cell. Infect. Microbiol.* 11:729981.  
doi: 10.3389/fcimb.2021.729981

<sup>1</sup> Department of Microbiology and Immunology, The Peter Doherty Institute for Infection and Immunity, University of Melbourne, Melbourne, VIC, Australia, <sup>2</sup> School of Chemistry and Molecular Biosciences, The University of Queensland, Brisbane, QLD, Australia, <sup>3</sup> Australian Infectious Diseases Research Centre, The University of Queensland, Brisbane, QLD, Australia, <sup>4</sup> Institute for Molecular Bioscience, The University of Queensland, Brisbane, QLD, Australia, <sup>5</sup> Department of Molecular and Biomedical Science, School of Biological Sciences, The University of Adelaide, Adelaide, SA, Australia, <sup>6</sup> School of Life Sciences, University of Technology Sydney, Ultimo, NSW, Australia, <sup>7</sup> School of Pharmacy and Biomedical Sciences, Curtin Health Innovation Research Institute, Curtin University, Bentley, WA, Australia

*Streptococcus pneumoniae* scavenges essential zinc ions from the host during colonization and infection. This is achieved by the ATP-binding cassette transporter, AdcCB, and two solute-binding proteins (SBPs), AdcA and AdcAll. It has been established that AdcAll serves a greater role during initial infection, but the molecular details of how the protein selectively acquires Zn(II) remain poorly understood. This can be attributed to the refractory nature of metal-free AdcAll to high-resolution structural determination techniques. Here, we overcome this issue by separately mutating the Zn(II)-coordinating residues and performing a combination of structural and biochemical analyses on the variant proteins. Structural analyses of Zn(II)-bound AdcAll variants revealed that specific regions within the protein underwent conformational changes *via* direct coupling to each of the metal-binding residues. Quantitative *in vitro* metal-binding assays combined with affinity determination and phenotypic growth assays revealed that each of the four Zn(II)-coordinating residues contributes to metal binding by AdcAll. Intriguingly, the phenotypic growth impact of the mutant *adcAll* alleles was, in general, independent of affinity, suggesting that the Zn(II)-bound conformation of the SBP is crucial for efficacious metal uptake. Collectively, these data highlight the intimate coupling of ligand affinity with protein conformational change in ligand-receptor proteins and provide a putative mechanism for AdcAll. These findings provide further mechanistic insight into the structural and functional diversity of SBPs that is broadly applicable to other prokaryotes.

**Keywords:** *Streptococcus pneumoniae*, zinc, solute-binding protein, ABC transporter, host-pathogen

## INTRODUCTION

Zinc is an essential micronutrient in all domains of life. Zinc, which occurs as the divalent cation Zn(II), fulfils both structural and functional roles within proteins, and is estimated to be required by up to 6% of the bacterial proteome (Andreini et al., 2006). Zinc serves in numerous essential cellular processes, such as DNA transcription and central carbon metabolism. Accordingly, Zn(II) acquisition is crucial for bacterial growth and virulence (Boylan et al., 2003; Hantke, 2005). The mammalian host exploits the essentiality of Zn(II) to control infection, by manipulating Zn(II) abundance and bioavailability (Hennigar and McClung, 2016). Nutritional immunity is the process wherein nutrients essential to infection by pathogens are withdrawn or have their bioavailability restricted. For Zn(II), this can be achieved by proteins such as human serum albumin (Lu et al., 2008; Cerasi et al., 2013) or the S100 family protein calprotectin, which is released from neutrophils (Kehl-Fie and Skaar, 2010). To overcome host-imposed Zn(II) restriction, pathogenic bacteria have evolved high-affinity acquisition systems to compete for metal ions at the host-pathogen interface (Ammendola et al., 2007; Sabri et al., 2009; Bayle et al., 2011; Pederick et al., 2015). These include the ubiquitous Type II ATP-binding cassette (ABC) family importers (Lewis et al., 2012), zinc-iron permease (ZIP) transporters (Grass et al., 2005; Karlinsey et al., 2010), P-type ATPases (Lewinson et al., 2009; Chien et al., 2013), and the recently identified zincophore scavenging systems (Lhospice et al., 2017; Morey and Kehl-Fie, 2020). Bacterial ABC permeases employ extra-cytoplasmic solute-binding proteins (SBPs) to obtain cargo such as Zn(II) ions from the periplasm (Gram-negative bacteria) or the extracellular environment (Gram-positive bacteria) (Lewis et al., 2012).

*Streptococcus pneumoniae* (the pneumococcus) is a leading bacterial cause of pneumonia and meningitis and is estimated to cause more than one million deaths annually (Weiser et al., 2018). As an obligate human pathogen, the pneumococcus is dependent on the host for nutrients (Henriques-Normark and Normark, 2010). The micronutrient Zn(II) is crucial for the pneumococcus to colonize and mediate disease in host tissues. Deletion of the Zn(II)-uptake machinery severely attenuates pneumococcal virulence (Plumptre et al., 2014). In *S. pneumoniae*, Zn(II) is primarily acquired *via* the ABC transporter AdcCB, which is comprised of a transmembrane domain (AdcB) and a nucleotide binding/hydrolyzing domain (AdcC), and two cluster A-I SBPs, AdcA and AdcAII (Dintilhac et al., 1997; Loisel et al., 2008). Both AdcA and AdcAII deliver Zn(II) to AdcCB, with either SBP sufficient for *in vitro* Zn(II) uptake (Bayle et al., 2011). However, murine studies show that both SBPs are required for full virulence *in vivo* with AdcAII contributing to a greater extent at the early stages of infection and invasive disease (Plumptre et al., 2014; Brown et al., 2016). Expression of the pneumococcal Zn(II) uptake machinery is principally controlled by the Zn(II)-dependent negative regulator AdcR, albeit to different extents (Plumptre et al., 2014). Notably, AdcAII is more highly upregulated than AdcA during growth in Zn(II)-restricted conditions (Reyes-Caballero et al., 2010; Plumptre et al., 2014). This is attributable to the distinct genetic location of *adcAII* and the presence of two AdcR binding sites upstream of the gene (Plumptre et al., 2014). AdcAII

is also co-expressed with the cell wall-localized Zn(II)-binding polyhistidine triad (Pht) proteins (Loisel et al., 2008; Plumptre et al., 2014). Studies show that AdcAII functions cooperatively with the Pht proteins to recruit Zn(II), but the mechanistic basis for how this occurs remains to be defined (Loisel et al., 2011; Bersch et al., 2013). Collectively, these observations have led to the proposal that AdcAII enhances Zn(II) uptake in metal-deficient niches, thereby aiding pneumococcal colonization and dissemination (Plumptre et al., 2014).

AdcAII belongs to the cluster A-I subgroup of SBPs, consisting of a conserved structural fold of two ( $\beta/\alpha$ )<sub>4</sub> domains connected by a rigid  $\alpha$ -helix, with the metal-binding site located at the interface between the N- and C-terminal lobes (Loisel et al., 2008; Yukl, 2017). Although both AdcA and AdcAII share this conserved fold, AdcA contains additional structural elements associated with Zn(II) recruitment (Plumptre et al., 2014). These are an extended C-terminal domain, which has homology to the Gram-negative Zn(II) chaperone ZinT, and a histidine-rich loop, which is common in Zn(II)-specific SBPs (Plumptre et al., 2014; Luo et al., 2021). AdcAII lacks these regions and although it does have a flexible loop of residues near the metal binding site, this loop is devoid of histidine residues (Wei et al., 2007; Loisel et al., 2008; Petrarca et al., 2010). Previous crystallographic studies of Zn(II)-specific SBPs from both Gram-positive and Gram-negative bacteria have shown only minor structural differences between the metal-free and Zn(II)-bound states (Chandra et al., 2007; Yatsunyk et al., 2008; Neupane et al., 2017; Luo et al., 2021). However, whether this fully represents the mechanistic diversity employed by Zn(II)-recruiting SBPs remains to be ascertained.

In this study, we investigated the Zn(II)-binding mechanism of AdcAII by mutating each of the four Zn(II)-coordinating residues in the SBP. The AdcAII mutant variants were then analyzed using a combination of biochemical, structural and molecular microbiology approaches. X-ray crystallographic analyses and molecular dynamics (MD) simulations showed that AdcAII samples a larger conformational landscape than other Zn(II)-specific SBPs reported to date. The binding site mutations impacted protein conformation and interaction with Zn(II) to differing extents. Surprisingly, phenotypic growth analyses of the AdcAII variants showed that perturbation of the Zn(II)-bound SBP conformation had a greater impact on *S. pneumoniae* growth in Zn(II)-limited media than relative affinity for Zn(II). Taken together, these data demonstrate the importance of SBP-metal complex conformation for bacterial Zn(II) uptake. Collectively, this study advances our mechanistic understanding of ligand recruitment by SBPs and uptake *via* the associated ABC transporter. This knowledge provides a foundation for future structure-based design of novel inhibitors targeting metal-ion uptake pathways.

## METHODS AND MATERIALS

### AdcAII Conservation Analysis

A global database of 20,020 publicly available *S. pneumoniae* genome sequences derived from the Global Pneumococcal

Sequencing project ([www.pneumogen.net](http://www.pneumogen.net)) (Gladstone et al., 2019) was assembled by the Wellcome Sanger Institute Pathogen Informatics pipeline (Page et al., 2016). The *Streptococcus pneumoniae* serotype 2 D39 genome (NCBI identifier NC\_008533) served as the reference genome to determine the presence, amino acid sequence and alignment of spd\_0888 (AdcAll) across the 20,020 clinical isolates using the screen\_assembly script (Davies et al., 2019) and BLASTN v2.9.0 with parameters of 80% coverage and 80% identity. For PspC and PspA, parameters of 50% coverage and 50% identity were used. Amino acid variation was determined using MUSCLE alignment in Geneious Prime (Kearse et al., 2012). Sequence conservation was determined by percentage of variant amino acids compared to consensus. Sequence conservation percentage was plotted against residue number in GraphPad Prism (Version 8). The alignment of non-redundant sequences was used to map residue conservation percentage onto Zn(II)-bound AdcAll (PDB ID: 3CX3) in UCSF Chimera *via* “render by conservation”.

## Bacterial Strains, Culturing and Growth Experiments

The mutant strain D39  $\Delta$ adcA was generated previously (Plumptre et al., 2014). Mutant strains in which wild-type *adcAll* was replaced with mutant variants were constructed using the Janus cassette (Sung et al., 2001). Briefly, the upstream and downstream flanking regions of *adcAll* were amplified using primers (**Supplementary Table 6**) with complementarity to the Janus cassette and were joined to the Janus cassette by overlap extension PCR. These linear fragments were used to replace *adcAll* in the chromosome of D39  $\Delta$ adcA mutant strains by homologous recombination. Successful transformants were identified *via* negative selection by virtue of growth on kanamycin and sensitivity to streptomycin. This strain, denoted D39  $\Delta$ adcA  $\Delta$ adcAll, was subsequently used to generate *adcAll* binding site mutants of *S. pneumoniae*. Exchange of the Janus cassette with mutant variants of *adcAll* was achieved by homologous recombination of mutant *adcAll* inserts previously combined with the upstream and downstream flanking regions of genomic *adcAll* by overlap extension PCR. *S. pneumoniae* wild-type and mutant strains (**Supplementary Table 5**) were routinely grown at 37°C with 5% CO<sub>2</sub> on blood agar (BA) [39 g/L Columbia base agar (Oxoid), 5% defibrinated horse blood] or THY [Todd-Hewitt broth (Oxoid), 0.5% w/v Bacto yeast extract]. Growth media were supplemented with antibiotics where appropriate: chloramphenicol (6  $\mu$ g.mL<sup>-1</sup>), streptomycin (150  $\mu$ g.mL<sup>-1</sup>), or kanamycin (50  $\mu$ g.mL<sup>-1</sup>). *E. coli* strains were routinely grown at 37°C in Luria Bertani Lennox broth (LB) or on LB 1.5% agar plates supplemented with kanamycin (50  $\mu$ g.mL<sup>-1</sup>) to maintain plasmids. For growth kinetic assays, *S. pneumoniae* strains were grown in a chemically defined medium (CDM; Dulbecco's modified Eagle medium base, 1  $\times$  BME vitamins, 74  $\mu$ M adenine, 89.2  $\mu$ M uracil, 65.7  $\mu$ M xanthine, 66.2  $\mu$ M guanine, 1123.5  $\mu$ M D,L-alanine, 757  $\mu$ M L-asparagine, 1127  $\mu$ M L-aspartic acid, 684.5  $\mu$ M L-glutamine, 1019.5  $\mu$ M L-glutamic acid, 868.6  $\mu$ M L-proline, 734.9  $\mu$ M L-tryptophan, 4125.4  $\mu$ M L-cysteine, 12  $\mu$ M lipoic acid, 1  $\mu$ M pyruvate; pH 7.4). Metal content of CDM was determined

by ICP-MS, as described previously (Neville et al., 2020). CDM routinely contained <1  $\mu$ M Zn(II) and <0.1  $\mu$ M Mn(II). *S. pneumoniae* strains were grown to mid-log (OD<sub>600</sub> = 0.3) in CDM supplemented with 1  $\mu$ M MnSO<sub>4</sub> and 10  $\mu$ M ZnSO<sub>4</sub>. Strains were then sub-cultured into 96-well microtiter plates to a final OD<sub>600</sub> of 0.05 in 200  $\mu$ L of CDM supplemented with varying concentrations of ZnSO<sub>4</sub>. Microtiter plates were sealed with gas permeable seals (Sigma Aldrich) and incubated at 37°C, 5% CO<sub>2</sub> in a CLARIOstar spectrophotometer (BMG Labtech), with measurements (OD<sub>600</sub>) recorded every 30 min for 16 h.

## Whole Cell Metal Ion Accumulation Analyses

Whole cell metal ion accumulation was determined by ICP-MS essentially as previously described (Plumptre et al., 2014). Briefly, *S. pneumoniae* strains were grown to mid-log phase (OD<sub>600</sub> = 0.3) in C+Y (per litre; 5 g yeast extract, 5 g casein hydrolysate, 6 mg L-tryptophan, 35 mg L-cysteine, 2 g sodium acetate, 8.5 g K<sub>2</sub>HPO<sub>4</sub>, 0.5 g MgCl<sub>2</sub>·6H<sub>2</sub>O, 2.5 mg CaCl<sub>2</sub>, 0.2  $\mu$ g biotin, 0.2 mg nicotinic acid, 0.2 mg pyridoxine-HCl, 0.2 mg thiamine-HCl, 0.1 mg riboflavin, 0.6 mg calcium pantothenate, 2 g glucose, and 12 mL 4% bovine serum albumin) supplemented with 1  $\mu$ M MnSO<sub>4</sub> and 10  $\mu$ M ZnSO<sub>4</sub>. Following three washes with 5 mM EDTA PBS and three washes with PBS, cells were harvested by centrifugation at 7,000  $\times$  g for 10 min and desiccated at 96°C for 18 h. Pellets were digested by treatment with 200  $\mu$ L of 65% HNO<sub>3</sub> at 96°C for 10 min, then diluted in MilliQ for metal-content analyses on an Agilent 8900 ICP-QQQ (Bio21, Melbourne).

## Expression and Purification of Recombinant AdcAll and Mutant Variants

Recombinant AdcAll (residues 35 – 311) was cloned from *S. pneumoniae* D39 genomic DNA (gene SPD\_0888) into pCAMcLIC01 *via* ligation independent cloning as previously described (McDevitt et al., 2011; Eijkelkamp et al., 2014). Mutant variants were generated by site-directed mutagenesis (QuikChange Lightning Kit, Agilent Technologies) using primers listed in **Supplementary Table 6**. Wild-type and mutant AdcAll variants were expressed in *E. coli* LEMO21(DE3) from their respective expression constructs (**Supplementary Table 7**). Expression cultures were grown in Overnight Express Instant TB medium (Merck) supplemented with 1% glycerol and 100  $\mu$ g.mL<sup>-1</sup> kanamycin for 18 h at 27°C. *E. coli* pellets were resuspended in 50 mM MOPS (pH 7.2), 200 mM NaCl, 20% glycerol, 15 mM imidazole buffer. Cells were homogenized with two Complete EDTA-free protease cocktail inhibitor tablets per 0.5 L of cells. Cells were mechanically disrupted using a Constant Systems Cell Disruptor at 30 kPSI. Cellular debris and membranes were removed *via* ultracentrifugation at 120,000  $\times$  g at 4°C for 1 h. Recombinant proteins were then purified *via* immobilized metal ion affinity chromatography. Soluble histidine-tagged protein was purified *via* three 5 mL HisTrap HP columns (GE Healthcare) connected in tandem. The dodecahistidine tag was removed from affinity-purified protein by enzymatic digestion by the human rhinovirus 3C protease and the protein was purified further on a HisTrap HP column. Metal-free protein was prepared by dialyzing the dodecahistidine tag-cleaved protein in a 20 kDa molecular

weight-cutoff (MWCO) membrane (Slide-A-Lyzer, ThermoFisher Scientific) against 4 L of sodium acetate (pH 5) buffer with 50 mM EDTA at 25°C for 24 h. The sample was then dialyzed against 4 L of 50 mM MOPS (pH 7.2), 200 mM NaCl buffer at 4°C for 24 h and centrifuged at  $18,000 \times g$  for 15 min to remove insoluble material. Protein samples were analyzed for metal content by heating 5  $\mu$ M protein at 96°C for 15 min in 3.5% HNO<sub>3</sub> with metal-ion content measured by ICP-MS. Protein samples were ultracentrifuged at  $204,428 \times g$  for 20 min to remove aggregating protein prior to biochemical analyses.

## Metal-Loading Analyses

Metal-free AdcAII (10  $\mu$ M; <10% metal content) was incubated with a molar excess of each metal – 10-fold for MnSO<sub>4</sub>, CoCl<sub>2</sub>, NiCl<sub>2</sub> and ZnSO<sub>4</sub>, and a 5-fold excess of CuSO<sub>4</sub>. Incubation of AdcAII with 10-fold for Cu(II) initially showed more than 2 Cu (II) atoms per molecule, despite AdcAII possessing only a single binding site. Accordingly, the molar excess of Cu(II) used in loading assays was reduced to minimize non-specific binding. Metal-loading assays were performed in 50 mM MOPS (pH 7.2) and 100 mM NaCl in a total volume of 2 mL, with samples incubated at 25°C for 30 min with agitation. Unbound metals were removed by desalting on a PD10 column (GE Healthcare). The metal:protein molar ratio was determined by ICP-MS using established methods (McDevitt et al., 2011).

## Differential Scanning Fluorimetry

Metal-free AdcAII (10  $\mu$ M; <10% metal content) was incubated with a 10-fold molar excess of MnSO<sub>4</sub>, FeSO<sub>4</sub>, CoCl<sub>2</sub>, NiCl<sub>2</sub>, CuSO<sub>4</sub> or ZnSO<sub>4</sub> at 25°C in the presence of 5  $\times$  SYPRO Orange (ThermoFisher Scientific) prior to thermal unfolding to 96°C at a heating rate of 0.1 °C.sec<sup>-1</sup> using a QuantStudio Flex 7 Real-Time PCR system (ThermoFisher Scientific). Fluorescence data were collected at Ex/Em 470/570 nm. Following subtraction of background fluorescence, the first derivative of the fluorescence data was determined and analyzed using GraphPad Prism (Version 8) to determine the  $T_m$ . Data were collected from at least three biological replicates.

## Competitive Zn(II) Binding Experiments

Fluorescence of 150 nM Mag-Fura-2 (ThermoFisher Scientific) (Ex/Em 340/510 nm) saturated with Zn(II) was measured on a CLARIOstar Plus spectrophotometer (BMG Labtech) at 25°C in response to increasing concentrations of metal-free protein. Five technical replicates of each sample were analyzed in a black half-volume 384-well microtiter plate (Greiner Bio One). All experiments were performed in Chelex-100 treated 50mM MOPS (pH 7.2) 200 mM NaCl buffer. Fluorescence values were analyzed using a one-site non-linear fit model in GraphPad Prism (Version 8) using the experimentally-derived  $K_D$  of Mag-Fura-2 (47 nM) to determine the  $K_D$  for Zn(II) binding by AdcAII.

## X-Ray Crystallography and Structure Determination

Mutant AdcAII proteins were purified to homogeneity and concentrated to approximately 10 mg.mL<sup>-1</sup> in centrifugal filter

units (Amicon MWCO 30 kDa, Millipore). Crystals were obtained at 18 - 20°C using the hanging drop vapor diffusion technique in the following conditions: AdcAII<sub>H65A</sub> and AdcAII<sub>E280Q</sub>, 0.1 M imidazole pH 8.0, 0.2 M zinc acetate, 20% (w/v) polyethylene glycol (PEG) 3350; AdcAII<sub>H205L</sub>, 0.2 M zinc acetate, 20% (w/v) PEG 3350. Crystals were mounted onto Cryoloops (Hampton Research) and briefly soaked in Paratone (Hampton Research) or 25%(v/v) glycerol prior to flash freezing in liquid nitrogen. X-ray diffraction data were collected at the Australian Synchrotron MX beamlines (McPhillips et al., 2002). Diffraction data were indexed and integrated using XDS (Kabsch, 2010) and scaled and merged using Aimless (Evans and Murshudov, 2013). Structures were determined using the molecular replacement technique in Phenix Phaser (Adams et al., 2010) using the crystal structure of wild-type AdcAII (PDB accession code: 3CX3) (Loisel et al., 2008) as the initial search model. Initial models were built in Phenix.AutoBuild (Terwilliger et al., 2008). The structures were refined iteratively using Phenix.Refine (Afonine et al., 2012) and manually modified in COOT (Emsley et al., 2010).

## Molecular Dynamics Simulations

Chain A in the crystal structure of Zn(II)-bound AdcAII (PDB-ID: 3CX3) was used as the starting structure for the wild-type AdcAII simulations. All crystallographic waters and sodium were removed. Missing atoms in the side chains of residues Thr142, Glu308, Glu309 and Lys253 were modelled using the side chains of other residues of the same type. The missing loop formed by residues 129-141 was reconstructed using the loop-building tool in SwissPDB Viewer (Guex and Peitsch, 1997). In the crystal structure, Zn(II) is coordinated by His65-N $\epsilon$ 2, His141-N $\epsilon$ 2, His205-N $\epsilon$ 2 and Glu280. Consequently, these His residues were modelled with a hydrogen atom on the ND1. All other His residues were protonated based on hydrogen bonding potential with surrounding residues.

For simulations of the AdcAII<sub>H65A</sub>, AdcAII<sub>H205L</sub> and AdcAII<sub>E280Q</sub> mutants, the crystal structures of Zn(II)-bound AdcAII<sub>H65A</sub>, AdcAII<sub>H205L</sub> and AdcAII<sub>E280Q</sub>, respectively, were used as starting structures. As before, missing atoms in the side chains or missing loops were reconstructed. The protonation state for all His residues was the same as in the simulations of wild-type AdcAII. For simulations of Zn(II)-free AdcAII and the equivalent mutants, the setup was identical except that the Zn(II) ion was removed from the crystal structure.

For all simulation systems, the protein was placed in a rectangular box, solvated with water molecules and Na<sup>+</sup> ions were added to neutralize the charge on the protein. Additional Na<sup>+</sup> and Cl<sup>-</sup> ions were added to obtain a final ionic strength of 100 mM NaCl. The system was energy-minimized using a steepest descent algorithm, followed by a 5 ns NPT run, where the protein backbone atoms were position-restrained with a force constant of 500 kJ mol<sup>-1</sup>.nm<sup>-2</sup>. For the wild-type protein as well as the three mutants, 750-ns NPT production simulations of the Zn-bound and Zn-free system, respectively, were run in duplicate (i.e. 4 proteins  $\times$  2 systems (metal-bound and metal-free)  $\times$  2 simulations for a total of 16 simulations). All simulations were carried out using the GROMACS package version 5.0.1 (Abraham et al., 2015) in conjunction with the

GROMOS 54a7 force field (Schmid et al., 2011) for protein and the simple point charge (SPC) model for water (Berendsen et al., 1981). Simulations were carried out under periodic boundary conditions with at least 1.5 nm between the protein and the box wall. Non-bonded interactions were described using a twin-range cut-off scheme with a 0.8 nm cut-off for short-range interactions and a 1.4 nm cut-off for long-range interactions. For long-range electrostatic interactions beyond 1.4 nm, a reaction field correction was applied, which was developed to be used for simulations with GROMACS and the GROMOS force field. A relative dielectric constant of  $\epsilon = 78.5$  was used. Covalent bonds were constrained using the SHAKE algorithm (Ryckaert et al., 1977), while the geometry of water molecules was constrained using the SETTLE algorithm (Miyamoto and Kollman, 1992). A Berendsen (Berendsen et al., 1984) thermostat with coupling constants of 0.1 ps was used to maintain the temperature close to the reference value of 25°C, while the Berendsen barostat with coupling constants of 0.5 ps was used for maintaining pressure close to 1 bar. Simulations were carried out using a 2-fs time step. Initial velocities were randomly assigned from Maxwellian distributions at 25°C. Configurations were saved every 500 ps for analysis. Analysis was carried out using GROMACS tools and the python library MDAnalysis (Michaud-Agrawal et al., 2011). Unless otherwise stated, only the last 250 ns of each trajectory was used for analysis and independent simulations for a given system were analyzed separately. All images were prepared using VMD (Humphrey et al., 1996). Cluster analysis was carried out using the algorithm of Daura et al. (Daura et al., 1999a; Daura et al., 1999b), implemented in GROMACS tools. A backbone neighbor RMSD cut-off of 2.5 Å was used. From each of the simulations, the most dominant conformation was used for comparison between metal-bound and metal-free states.

## Data Availability

The accession codes for the structures deposited in the Protein Data Bank are: 7LM5 (Zn<sup>2+</sup>-bound AdcAII<sub>H65A</sub>), 7LM6 (Zn<sup>2+</sup>-bound AdcAII<sub>H205L</sub>), and 7LM7 (Zn<sup>2+</sup>-bound AdcAII<sub>E280Q</sub>).

## RESULTS

### AdcAII Is Highly Conserved in *S. pneumoniae*

The conservation of AdcAII was assessed by comparing the amino acid sequence of AdcAII (SPD\_0888) across 20,020 *S. pneumoniae* genomes. This revealed that AdcAII had 99.97% prevalence and 99.25% conservation across all genomes, comparable to conservation and prevalence levels of the multilocus sequence typing genes *aroE*, *gdhA*, *gki*, *ddl*, and *xpt* (Supplementary Table 1). Non-redundant sequence conservation analysis showed that 295 of 306 residues in AdcAII were more than 95% conserved between the 20,016 strains carrying *adcAII* (Supplementary Figure 1A). The Zn(II)-coordinating residues were absolutely conserved (100%) in all strains, and only four residues were found to have less than 80% conservation (Supplementary Figure 1B). The high level of conservation maintained in AdcAII contrasts with other major surface proteins involved in

virulence and disease, such as PspC and PspA, which despite sharing the same cellular localization, show significantly lower prevalence and conservation (Supplementary Table 1). These data suggest that mutations that perturb the Zn(II)-coordinating site or alter global protein structure are poorly tolerated in AdcAII. It therefore follows that the conservation of AdcAII and its Zn(II)-recruiting function are important for pneumococcal survival.

### Zinc Binding Induces Localized Structural Changes in AdcAII

We next sought to investigate the structure and Zn(II)-binding mechanism of AdcAII. First, we attempted to crystallize metal-free AdcAII, to determine the structure of the open, ligand-free state. Although crystals of metal-free AdcAII were obtained, they had a diffraction limit of 4 Å resolution, with poorly resolved electron density maps, and structure determination was not pursued further. Nevertheless, the domain-linking helix region (residues 168–194) could be built into the electron density map (data not shown). This suggested that in the absence of Zn(II) stabilization, there may be complexity within the conformational landscape of the protein. This may arise from the N- and C-terminal lobes, or discrete regions therein, exhibiting mobility/flexibility and/or adopting distinct conformational positions in the absence of the metal ion. We speculated that these regions within AdcAII could be restrained, and a partially open conformation achieved by mutating each of the four Zn(II)-coordinating residues: His65, His141, His205 and Glu280. For this, the Zn(II)-coordinating residues were substituted with an uncharged residue. Alanine was substituted for His65, which has recently been implicated as a component of a crucial mobile loop in *S. pneumoniae* AdcA (Luo et al., 2021), and His141. Leucine and glutamine were substituted for residues His205 and Glu280, respectively, to preserve steric bulk. Here, we report the crystal structures of the mutant variants in the Zn(II)-bound state: Zn-AdcAII<sub>H65A</sub> (PDB: 7LM5), Zn-AdcAII<sub>H205L</sub> (PDB: 7LM6), and Zn-AdcAII<sub>E280Q</sub> (PDB: 7LM7). Although the AdcAII<sub>H141A</sub> mutant variant was generated, it was refractory to structure determination. Detailed crystallography data statistics for the AdcAII variants are summarized in Supplementary Table 2.

The AdcAII variant crystal structures all show a canonical cluster A-I SBP fold similar to the previously reported structure of wild-type Zn(II)-bound AdcAII [Zn-AdcAII; (Loisel et al., 2008)] (Supplementary Figure 2). Despite the absence of one of the metal-coordinating residues, each of the variants contained a single Zn(II) atom at the metal-binding site (Supplementary Figure 3). Coordination bond lengths of approximately 2.1 Å were observed in all structures, indicative of typical Zn(II)-protein binding. The C $\alpha$ -C $\alpha$  root-mean-square deviations (RMSDs) between Zn-AdcAII and Zn-AdcAII<sub>H65A</sub>, Zn-AdcAII<sub>H205L</sub> and Zn-AdcAII<sub>E280Q</sub> were 0.44, 0.66 and 0.47 Å, respectively, indicating no major deviation in main chain conformation. Nevertheless, significant differences were observed by comparison with Zn-AdcAII. Notably, Zn-AdcAII adopts a conformation wherein the metal-binding site is fully occluded from solvent, whereas Zn-AdcAII<sub>H65A</sub> and Zn-AdcAII<sub>H205L</sub> showed distinct surface conformations in the N- and C-terminal lobes, respectively. In the Zn-AdcAII<sub>H65A</sub>

structure, electron density for the  $\alpha 2\beta 2$  loop (residues 60-67) was not observed, suggesting that the loop is more mobile in the absence of Zn(II) and stabilized by Zn(II) coordination *via* His65 (**Figure 1A**), as was recently implicated in structural analysis of AdcA (Luo et al., 2021). Thus, mutation of His65 resulted in exposure of the bound Zn(II) ion to bulk solvent on the N-terminal side of the binding site. The structure of Zn-AdcAII<sub>H205L</sub> also showed noticeable deviation from the Zn-AdcAII structure, with the differences primarily localized to the C-terminal lobe of the protein (**Figure 1B**). These manifested as rotation of helices  $\alpha 7$  ( $32^\circ$ ) and  $\alpha 8$  ( $28^\circ$ ); loss of H-bonding between  $\beta$ -strands  $\beta 5$  and  $\beta 6$ ; and disorder for part of loop  $\alpha 7\beta 6$  (residues 223-233), as evidenced by the lack of electron density in this region. These changes suggest that metal coordination by His205 facilitates formation of the  $\beta 5$ - $\beta 6$  interface, resulting in the movement of loop  $\alpha 7\beta 6$  and subsequent rotation of helices  $\alpha 7$  and  $\alpha 8$ . Notably, as loop  $\alpha 7\beta 6$  shields the entrance of the metal-binding site, its absence exposes the bound Zn(II) to bulk solvent from the C-terminal lobe. Thus, loops  $\alpha 7\beta 6$  and  $\alpha 2\beta 2$  seem to serve as the gating loops of the metal-binding site, with Zn(II)-binding directly coupling to the closure of the metal binding site.

Finally, structure determination of Zn-AdcAII<sub>E280Q</sub> revealed negligible global differences by comparison with Zn-AdcAII, with the metal-binding site and bound Zn(II) ion occluded from solvent (**Figure 1C**). The point mutation appeared to preclude Gln280 interaction with Zn(II), with the O $\epsilon$ 1 atom  $\sim 4.4$  Å distant from the metal. In wild-type AdcAII the Glu280 O $\epsilon$ 2 atom contributed to the coordination of the metal ( $\sim 2.3$  Å from the Zn(II) ion) as the O $\epsilon$ 1 atom was outside of the ideal range for interaction ( $\sim 3.2$  Å from the Zn(II) ion). Taken together, these data indicate that coordination of the Zn(II) by Glu280 does not appear to play a major role in the conformational changes. Thus, the role of residue Glu280 appears to be in completing the metal coordination sphere and

reducing the solvent accessibility of the metal-binding site in the Zn(II)-bound state. Collectively, structural analyses of AdcAII variant proteins show that metal-binding by His65 and His205 is directly coupled to protein conformational changes. These were not observed for Glu280, while His141 remained refractory to this approach.

## Molecular Dynamics Simulations of AdcAII and Mutant Variants

Building on the structural insights into AdcAII and the mutant variants, molecular dynamics (MD) simulations were used to further study the SBP. First, MD simulations were performed on metal-free and Zn(II)-bound wild-type AdcAII. Simulations for the Zn(II)-bound wild-type AdcAII were set up using the corresponding crystal structure. Due to the lack of a metal-free structure, Zn(II)-bound AdcAII with the metal ion removed was used as a starting structure. Metal-free and Zn(II)-bound states of wild-type AdcAII were simulated for 750 ns in duplicate. For all analyses, the last 250 ns of the relevant trajectories were used. Cluster analysis on all backbone atoms with a cut-off = 2.5 Å was used to identify the dominant conformations sampled in the simulations of metal-free and Zn(II)-bound wild-type AdcAII. Comparison of these structures indicates that the global protein fold is not affected by the presence of Zn(II), suggesting that no large-scale structural rearrangements are triggered by AdcAII-metal binding. In addition, no significant differences in the root-mean square fluctuations (RMSF) between Zn(II)-bound and metal-free states were observed. This suggested that the overall mobility of different protein domains remains unchanged in the presence and absence of Zn(II) (**Supplementary Figure 4A**). To further assess conformational differences between the two states of the protein, the average pairwise C $\alpha$ -C $\alpha$  distances were calculated between all possible residue pairs over 250 conformations, for each respective simulation. The differences between each C $\alpha$ -C $\alpha$  distance in the Zn(II)-bound and metal-

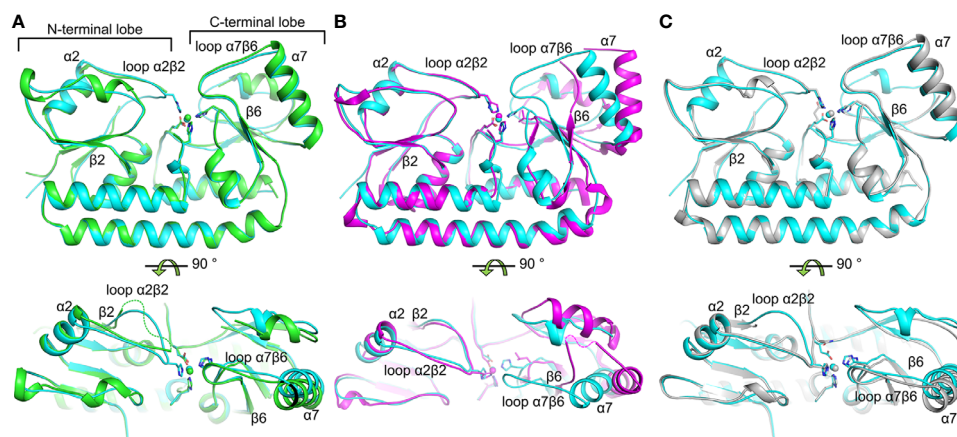


**FIGURE 1** | Structural comparisons of *S. pneumoniae* AdcAII wild-type and mutant variants. **(A–C)** depict the superposition of crystal structures of the wild-type Zn(II)-bound AdcAII (PDB ID: 3CX3, cyan) and AdcAII<sub>H65A</sub> (PDB ID: 7LM5, green), AdcAII<sub>H205L</sub> (PDB ID: 7LM6, magenta), and AdcAII<sub>E280Q</sub> (PDB ID: 7LM7, grey), respectively. The bound Zn(II) ions are shown as spheres and their coordinating residue side chains as sticks. Missing loops in **(A, B)** are indicated by dotted lines in the bottom panels.

free state was then determined ( $\Delta_{C\alpha-C\alpha}$  distance). The  $\Delta_{C\alpha-C\alpha}$  distances provide insight into regions of the protein that adopt different conformations in the metal-free state relative to the Zn(II)-bound state of the protein. This revealed that loop  $\alpha 2\beta 2$ , which contains the metal-binding site residue His65, adopted different relative positions in simulations of the two states (**Figures 2A, B**). Quantification of changes between the metal-free and Zn(II)-bound simulations was performed by RMSD vs. time analysis (**Figures 2C–F**). This revealed that only loop  $\alpha 2\beta 2$  showed a significant difference in comparison of the two states (99% confidence interval). The three loops that contain each of the other metal-coordinating residues – loop  $\alpha 3\beta 4$  (His141); loop  $\alpha 6\beta 5$  (His205); and loop  $\alpha 9\beta 8$  (Glu280) – showed much lower differences between the metal-free and Zn(II)-bound simulations (68% confidence interval). Analysis further showed that in the metal-free state, loop  $\alpha 2\beta 2$  moved away from its

original position within the first ~100 ns of the simulation and remained in this same position for the rest of the simulation. On the other hand, loop  $\alpha 7\beta 6$ , which was predicted to be stabilized upon Zn(II) coordination by His205 from the Zn-AdcAII<sub>H205L</sub> crystal structure, showed a much less pronounced increase in mobility in the absence of Zn(II). This suggests that of the four loops that contain the metal-binding residues, loop  $\alpha 2\beta 2$  shows the most pronounced change in conformation upon Zn(II) binding.

In addition to the simulations of wild-type AdcAII, we performed MD simulations on the AdcAII variants AdcAII<sub>H65A</sub>, AdcAII<sub>H205L</sub> and AdcAII<sub>E280Q</sub> (**Supplementary Figures 4B, 5**). For the Zn(II)-bound simulations, the corresponding crystal structures were used. As performed for the wild-type, the metal-free systems were setup by removing the metal from the Zn(II)-bound structure. For all three variants,

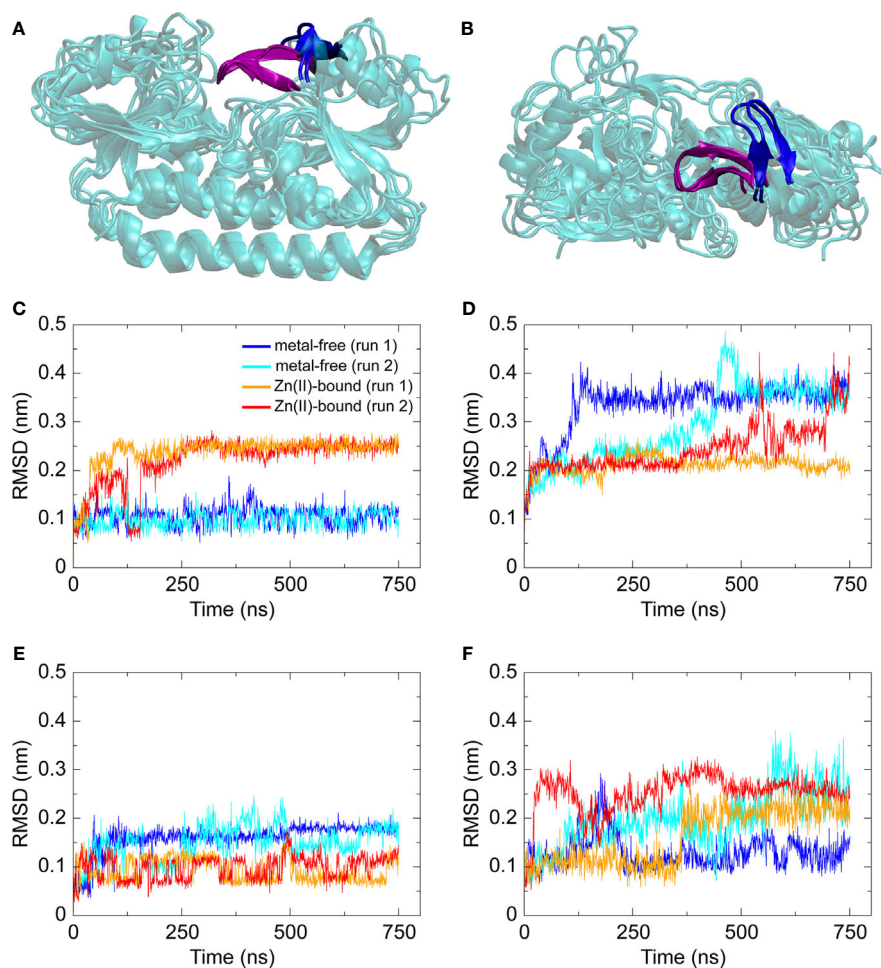


**FIGURE 2** | Structures and RMSD vs. time data from MD simulations of Zn(II)-bound and metal-free wild-type AdcAII. **(A, B)** Dominant conformations, as determined by clustering analysis, from duplicate simulations of metal-free and Zn(II)-bound AdcAII. The protein is shown in cartoon representation in cyan. Loop  $\alpha 2\beta 2$ , which contains His65, is shown in purple for the Zn(II)-bound state and in blue for the metal-free state. **(C–F)** RMSD (nm) vs. time (ns) data for the four metal-coordinating loops – loop  $\alpha 2\beta 2$  containing His65 **(C)**, loop  $\alpha 3\beta 4$  containing His141 **(D)**, loop  $\alpha 6\beta 5$  containing His205 **(E)**, and loop  $\alpha 9\beta 8$  containing Glu280 **(F)** – calculated from duplicate ( $n = 2$ ) 750 ns simulations of metal-free and Zn(II)-bound AdcAII. For all four plots, data from each simulation (two metal-free, two Zn(II)-bound) state are shown and color-coded as denoted in **(C)**.

simulations of metal-free and Zn(II)-bound states were carried out for 750 ns, in duplicate, with the last 250 ns used for analysis. Analysis of the AdcAII<sub>H205L</sub> and AdcAII<sub>E280Q</sub> variants revealed no significant differences in residue position or mobility between the metal-free and Zn(II)-bound simulations, the latter of which is consistent with the minimal structural changes observed in the Zn-AdcAII<sub>E280Q</sub> structure (**Supplementary Figure 5; Supplementary Tables 3, 4**). Simulations of AdcAII<sub>H205L</sub> showed that changes in the C-terminal lobe were attributable to the untethering of His205 from the metal-binding site and the inability to form the  $\beta 5$ - $\beta 6$  interface. An additional 750 ns simulation was conducted on Zn(II)-bound AdcAII<sub>H205L</sub> with analyses revealing that, in two (of the three) independent simulations, Zn(II) moves out of its solvent-exposed metal binding site. Thus, the MD simulations support inferences from the crystal structure that the role of loop  $\alpha 7\beta 6$  is to reduce bulk solvent access to the metal-binding site mediated *via* Zn(II)-coordination with His205.

Simulations of AdcAII<sub>H65A</sub> revealed that in the metal-free state, loop  $\alpha 2\beta 2$  and helix  $\alpha 2$  adopt unique conformations that are not observed in the Zn(II)-bound state of the AdcAII<sub>H65A</sub> variant or in either state of wild-type AdcAII (**Supplementary Figure 4B**). As noted above, the Zn-AdcAII<sub>H65A</sub> crystal structure did not show electron density for the  $\alpha 2\beta 2$  loop (residues 60-67), which indicates this loop has greater mobility in the variant protein than the wild-type. However, this does not imply that  $\alpha 2\beta 2$  loop is disordered as the lack of electron density can arise from the loop adopting multiple distinct conformations. While these conformations would be refractory to crystallographic

approaches, they can be captured by the MD simulations. When considered in context with the Zn-AdcAII<sub>H65A</sub> structure, these data suggest that loop  $\alpha 2\beta 2$  controls access to the N-terminal side of the metal-binding site, with its conformation being restricted by interaction of His65 with the Zn(II) ion. Intriguingly, the loop  $\alpha 2\beta 2$  region was recently shown to be critical for the function of AdcA for *S. pneumoniae* Zn(II) uptake in a  $\Delta$ adcAII background (Luo et al., 2021). However, the high mobility and dynamic conformational sampling of loop  $\alpha 2\beta 2$  in the metal-free state of AdcA is distinctly different from the equivalent region in AdcAII (**Figure 3**). In AdcA, loop  $\alpha 2\beta 2$  adopts different conformations in the two states of the protein, with the region demonstrating high mobility in the absence of the Zn(II). By contrast, although loop  $\alpha 2\beta 2$  adopts different conformations in the Zn(II)-bound and metal-free states of AdcAII, the loop does not exhibit dynamic mobility. This suggests that despite sharing similar global architectures, there are subtle conformational and mechanistic differences in the Zn(II)-binding mechanism of these two SBPs. Collectively, our biophysical analyses of AdcAII and its binding-site mutant derivatives strongly suggest that loops  $\alpha 2\beta 2$  and  $\alpha 7\beta 6$  are involved in conformational changes upon Zn(II) binding.

### Metal-Binding Properties of Wild-Type AdcAII and Mutant Variants

To further probe the role of each Zn(II)-coordinating residue in AdcAII, we examined the metal-binding properties of the protein using *in vitro* metal-loading experiments, differential scanning

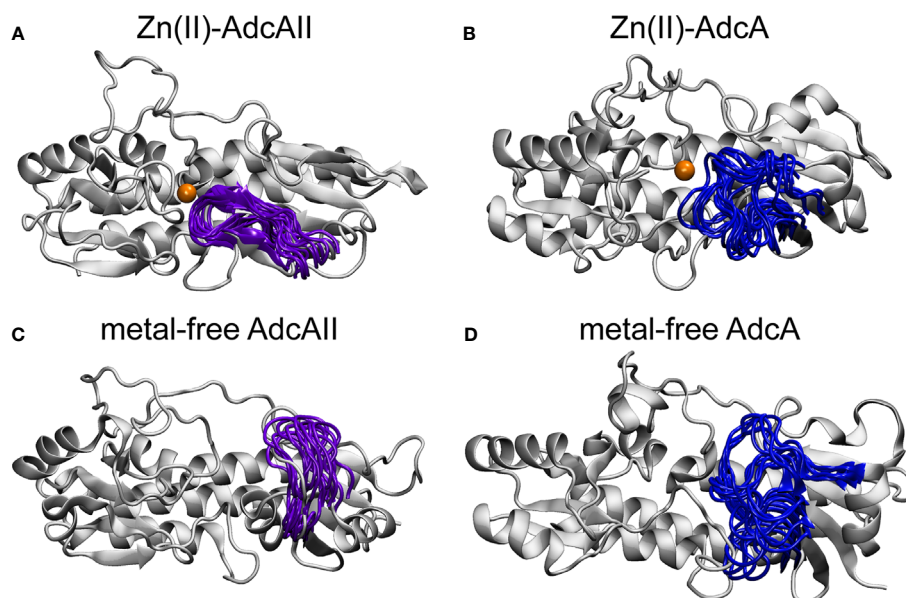


**FIGURE 3** | Comparison of  $\alpha 2\beta 2$  loop in AdcAII and the AdcA N-terminal cluster A-I domain. Conformation of  $\alpha 2\beta 2$  loop in AdcAII (**A, C**) and AdcA (**B, D**), in the Zn(II)-bound (**A, B**) and metal-free (**C, D**) states. The protein is shown in cartoon representation in grey with the  $\alpha 2\beta 2$  loop shown in purple (AdcAII) and dark blue (AdcA). The Zn(II) ion is shown in orange. Conformations for the movement of the  $\alpha 2\beta 2$  loop are taken from conformations of duplicate 750-ns simulations of the AdcAII and A-I AdcA domain.

fluorimetry (DSF), and affinity determination assays. *In vitro* metal-loading of AdcAII assessed binding of metal ions by inductively coupled plasma-mass spectrometry (ICP-MS). Wild-type AdcAII bound  $0.89 \pm 0.07$  Zn(II) atoms per molecule, consistent with a single metal-binding site (Loisel et al., 2008). AdcAII was also shown to be permissive for interaction with the first-row transition metal ions Mn(II), Co(II), Ni(II) and Cu(II), albeit to varying extents (**Figure 4A**). Variation in the extent of the metal-bound states can most likely be attributed to cation dissociation due to sample washing prior to ICP-MS analysis. The metal-binding behavior of AdcAII was in stark contrast to AdcA, which is highly specific for Zn(II) and does not appreciably interact with other divalent cations (Plumptre et al., 2014; Luo et al., 2021). We then examined the *in vitro* Zn(II)-binding of the AdcAII mutant variants, to understand the impact of the mutations on interaction with the physiological ligand. *In vitro* binding of Zn(II) was severely impaired in AdcAII<sub>H141A</sub>, significantly reduced in AdcAII<sub>H65A</sub> and AdcAII<sub>E280Q</sub>, but not significantly affected in AdcAII<sub>H205L</sub> (**Figure 4B**). Collectively, these data demonstrate that AdcAII is not restricted to interacting solely with Zn(II), despite extensive evidence (Loisel et al., 2008; Bayle et al., 2011; Bersch et al., 2013; Plumptre et al., 2014; Brown et al., 2016) indicating that it is the primary physiological ligand. Further, mutation of the metal binding site residues impacts Zn(II) binding, albeit to different extents.

We then analyzed wild-type AdcAII and the mutant variants by DSF, to ascertain how metal-protein interactions influenced SBP thermostability. In wild-type AdcAII, Zn(II) and Co(II) induced significant melting temperature ( $T_m$ ) shifts, Mn(II), Ni(II), and Cu(II) induced smaller, but still significant,  $T_m$  increases, while Fe(II) did not significantly alter the  $T_m$  (**Table 1**). These data suggest that the metal-binding site of AdcAII can interact to some degree with the majority of first row transition metal ions, consistent with the ICP-MS results. Nevertheless, the thermostability shifts observed were relatively small for cations

other than Co(II) or Zn(II). We speculate that differences in coordination of the non-cognate cations at the AdcAII metal-binding site is most likely attributable for the variations in observed thermostabilities of protein-metal complexes. Whether the interaction with other cations can facilitate productive import is unclear. To date, the contribution, if any, of the AdcCB importer to regulating metal import remains undefined. Future studies to address this question would also need to consider the contribution of the *S. pneumoniae* metal export systems MntE, CopA, and CzcD.

DSF analyses of the AdcAII mutant variants revealed that the binding site mutations had no effect on the thermostability of the proteins in the metal-free state, by comparison with the wild-type protein (**Table 2**). This indicates that the binding site mutations do not destabilize the global protein structure of the SBPs. DSF analysis of the AdcAII variants with the cognate ligand showed a significant reduction in the  $\Delta T_m$  of all variants (**Table 2**). Zn(II)-AdcAII<sub>H141A</sub> showed the lowest  $\Delta T_m$ , with a reduction of 18.75 °C relative to wild-type protein. This was followed by Zn(II)-AdcAII<sub>H65A</sub> and Zn(II)-AdcAII<sub>H205L</sub>, which showed similar  $\Delta T_m$  reductions of 16.56 °C and 13.16 °C, respectively, by comparison with wild-type AdcAII, while in Zn(II)-AdcAII<sub>E280Q</sub>, the  $\Delta T_m$  was reduced by only 9.91°C relative to the wild-type protein. In summary, the DSF analyses show that all four of the metal-coordinating residues contribute to ligand-induced stabilization of AdcAII. Accordingly, we sought to further investigate the impact of the binding site mutations by determining the affinity of wild-type AdcAII and the variants for Zn(II).

The dissociation constant ( $K_D$ ) of AdcAII for Zn(II) was determined using a competitive binding assay with the metal-responsive fluorophore MagFura-2. Wild-type AdcAII bound Zn(II) with an experimentally derived  $K_D$  of  $18.7 \pm 2.1$  nM (**Table 3** and **Supplementary Figure 6**) and is within the sub-nanomolar to micromolar range of previously characterized Zn(II)-specific cluster A-I SBPs (Desrosiers et al., 2007; Wei et al., 2007; Lim

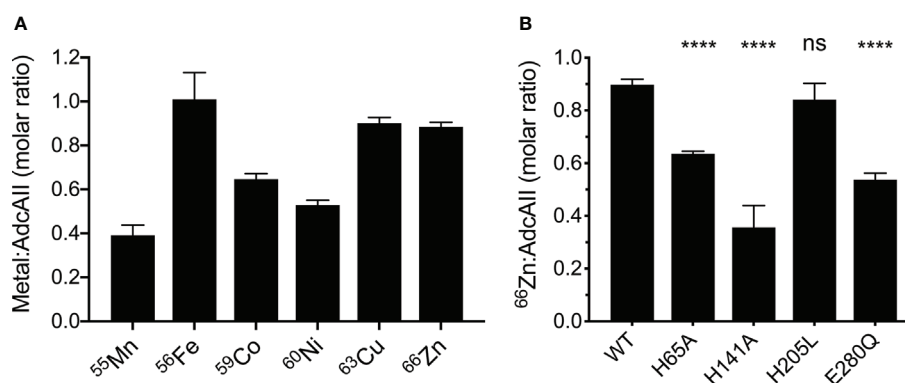


**FIGURE 4** | Biochemical analyses of recombinant wild-type AdcAII and mutant variants. **(A)** *In vitro* metal-binding experiments of metal-free AdcAII with first-row transition metal ions are shown. Data represent the mean molar ratio of metal to AdcAII ( $\pm$  SEM) determined by ICP-MS from at least three independent biological experiments. **(B)** *In vitro* Zn(II)-binding experiments of AdcAII mutant variants AdcAII<sub>H65A</sub>, AdcAII<sub>H141A</sub>, AdcAII<sub>H205L</sub> and AdcAII<sub>E280Q</sub> analyzed by ICP-MS. Data represent the mean molar ratio of metal to protein ( $\pm$  SEM) from at least three independent biological experiments. Statistical analyses comparing mutant variants to the wild-type protein were performed by one-way ANOVA with Tukey post-test with  $P$ -values of  $> 0.05$  and  $< 0.0001$  are denoted by ns and \*\*\*\*, respectively.

**TABLE 1** | Effect of transition metal ions on the melting temperature of AdcAII.

Treatment	$T_m$ (°C) <sup>a</sup>	$\Delta T_m$
Metal-free	51.01 ± 0.16	–
Mn(II)	54.96 ± 0.34 <sup>b</sup>	+3.95
Fe(II)	53.09 ± 0.24	+2.20
Co(II)	70.08 ± 2.19 <sup>b</sup>	+19.08
Ni(II)	57.15 ± 0.24 <sup>b</sup>	+6.14
Cu(II)	60.48 ± 0.66 <sup>b</sup>	+9.38
Zn(II)	75.92 ± 0.57 <sup>b</sup>	+24.91

a. Values shown represent the average and standard error of the mean from at least 3 independent measurements.

b. Statistically significant difference to metal-free protein  $T_m$  (one-way ANOVA with Tukey post-test).

et al., 2008; Plumptre et al., 2014; Handali et al., 2015). Affinity determination for the AdcAII variants revealed that all mutants had reduced affinity for Zn(II) relative to wild-type AdcAII and followed the order of: AdcAII > AdcAII<sub>H205L</sub> > AdcAII<sub>E280Q</sub> > AdcAII<sub>H65A</sub> > AdcAII<sub>H141A</sub> (Table 3 and Supplementary Figure 6). These data show that mutation of His141 compromised interaction of AdcAII with Zn(II) to the greatest extent, consistent with the refractory nature of the mutant SBP to structure determination. Mutation of either Glu280 or His65 resulted in mutants compromised to similar extents with respect to interaction with Zn(II). Intriguingly, although mutation of His205 reduced the thermostability of the SBP-metal complex and resulted in displacement of the C-terminal lobe of the protein, the AdcAII<sub>H205L</sub> variant showed higher affinity for Zn(II) and a greater capacity to retain the bound ion compared with the other mutants. Taken together, these data suggest that AdcAII<sub>H205L</sub> is capable of efficient Zn(II) recruitment but would likely be compromised for efficacious uptake due to the inability of the SBP to transition to a closed conformation. Accordingly, we investigated how the binding site mutations affected Zn(II) acquisition by the Adc permease in *S. pneumoniae*.

## Conformational Changes in AdcAII Are Required for Efficacious Zinc Uptake

The impact of the binding site mutations on pneumococcal Zn(II) uptake was addressed by generating mutant *S. pneumoniae* strains in the D39  $\Delta$ adcA background (Plumptre et al., 2014), which excluded the contribution of AdcA to Zn(II) import (Supplementary Table 5). Growth kinetics and zinc uptake in the *S. pneumoniae* *adcAII* mutant strains were then assessed in

**TABLE 2** | Effect of zinc on the melting temperature of AdcAII binding site variants.

	Metal-free $T_m$ (°C) <sup>a</sup>	Zn(II) $T_m$ (°C)	$\Delta T_m$ (°C)
WT AdcAII	51.01 ± 0.16	75.92 ± 0.57 <sup>b</sup>	+24.91
H65A	51.52 ± 0.61	59.86 ± 0.78 <sup>b</sup>	+8.35 <sup>c</sup>
H141A	49.11 ± 0.69	54.99 ± 0.87 <sup>b</sup>	+6.16 <sup>c</sup>
H205L	49.90 ± 0.37	61.65 ± 0.64 <sup>b</sup>	+11.75 <sup>c</sup>
E280Q	50.31 ± 0.54	65.31 ± 1.02 <sup>b</sup>	+15.00 <sup>c</sup>

a. Values shown represent the average and standard error of the mean from at least 3 independent measurements.

b. Statistically significant difference to metal-free protein  $T_m$  (one-way ANOVA with Tukey post-test).

c. Statistically significant difference to WT AdcAII  $\Delta T_m$  (unpaired t-test,  $P < 0.0001$ ).

cation-defined minimal media (CDM), while whole cell metal accumulation studies used Zn(II)-replete (10  $\mu$ M) C+Y medium. This latter variation was necessitated by the poor biomass recovery of CDM grown cultures for whole cell metal accumulation analyses, which was overcome by use of C+Y growth medium. The *S. pneumoniae* wild-type and  $\Delta$ adcA strain showed similar levels of Zn(II) accumulation, consistent with prior studies (Figure 5A) (Plumptre et al., 2014). Although the *S. pneumoniae* *adcA* *adcAII* double knockout strain ( $\Delta$ adcA *adcAII::Janus*) grew, it failed to generate sufficient biomass for metal content determination. The *S. pneumoniae* strains encoding the *adcAII* binding site mutants revealed that all strains had significantly reduced Zn(II) accumulation relative to the parental strain (Figure 5A). However, there was no significant difference in Zn(II) accumulation between the individual mutant strains. This indicated that all strains acquired sufficient Zn(II) for viability in Zn(II)-replete C+Y, but there was insufficient resolution using this growth medium to assess any differences between the strains. To further investigate differences between strains, we employed Zn(II)-depleted CDM that contained less than 200 nM Zn(II).

The *S. pneumoniae* wild-type and  $\Delta$ adcA strain showed similar growth phenotypes in CDM, while the double mutant,  $\Delta$ adcA *adcAII::Janus*, was greatly attenuated (Figure 5B). The *S. pneumoniae*  $\Delta$ adcA *adcAII*<sub>H141A</sub> complemented strain ( $\Delta$ adcA  $\Omega$ adcAII<sub>H141A</sub>) demonstrated very poor growth in CDM, consistent with the impact of the mutation observed in our other analyses. The  $\Delta$ adcA  $\Omega$ adcAII<sub>H65A</sub> strain showed a minor defect in growth, while the growth phenotype of the  $\Delta$ adcA  $\Omega$ adcAII<sub>E280Q</sub> strain was comparable to the wild-type and parental strains. These data indicate that the impact of the binding site mutations on AdcAII Zn(II) affinity only manifests itself as a modest effect on bacterial Zn(II) uptake and growth in Zn(II)-restricted conditions. Intriguingly, the growth phenotype of the  $\Delta$ adcA  $\Omega$ adcAII<sub>H205L</sub> strain was perturbed to a greater extent than the strains harboring either the His65 or Glu280 mutations. All *S. pneumoniae* binding site mutant strains demonstrated a growth phenotype comparable to the wild-type strain when supplemented with 10  $\mu$ M Zn(II) (Figure 5C). These data show that despite the AdcAII<sub>H205L</sub> variant retaining a higher affinity for Zn(II), this is not sufficient for optimal growth in Zn(II)-restricted conditions. It therefore follows that the inability of the AdcAII<sub>H205L</sub> variant to support optimal *S. pneumoniae* growth is due to another impact of the mutation. The AdcAII<sub>H205L</sub> structure shows that the mutant variant is unable to transition to a closed conformation with the C-terminal lobe essentially ‘untethered’ from the metal-binding site. Therefore, we speculate that the inability to adopt

**TABLE 3** | Effect of metal binding site mutations on *in vitro* Zn(II) binding.

AdcAII variant	Dissociation Constant $K_D$ (nM)
WT AdcAII	18.7 ± 2.1
AdcAII <sub>H65A</sub>	174.4 ± 30.7
AdcAII <sub>H141A</sub>	247.8 ± 63.8
AdcAII <sub>H205L</sub>	44.7 ± 3.6
AdcAII <sub>E280Q</sub>	159.3 ± 42.7

the metal-bound, closed conformation, impairs Zn(II) uptake in the  $\Delta\text{adcA } \Omega\text{adcAII}_{\text{H205L}}$  strain. However, the dynamics of Zn(II) release from AdcAII, how this is affected in mutant variants, and the impact of the mutation(s) on AdcB-AdcAII interaction likely also contribute and warrant further investigation to comprehensively understand the mechanisms of Zn(II) uptake *via* the Adc permease.

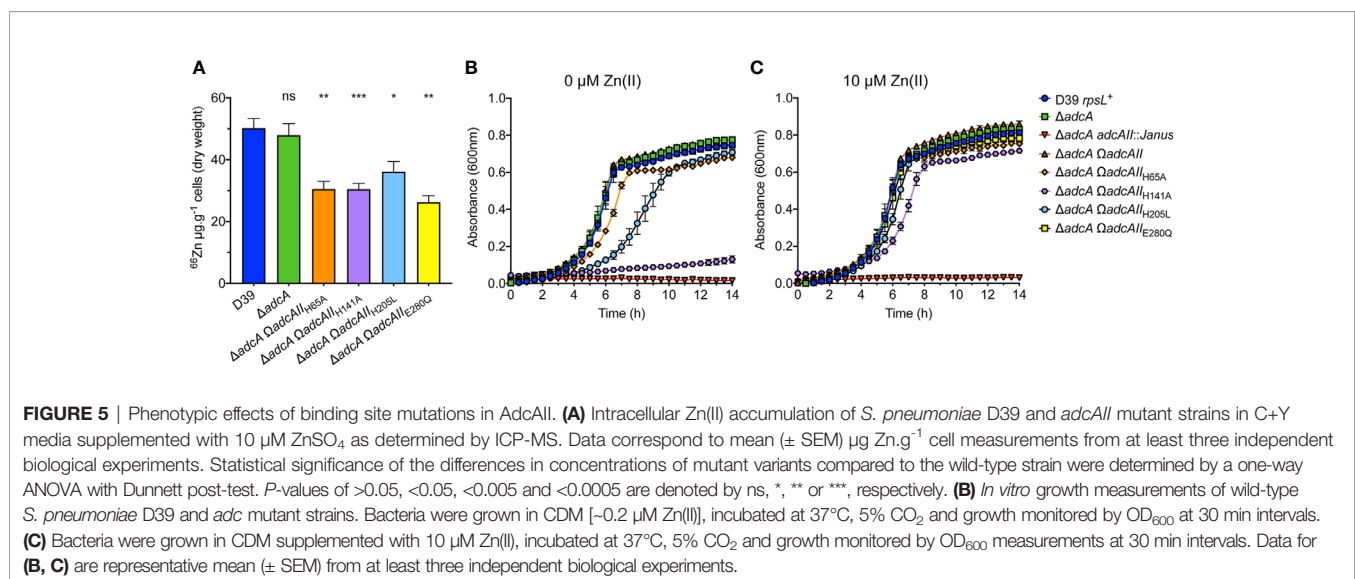
## Proposed Zn(II)-Binding Mechanism of AdcAII

Our analyses of AdcAII reveal that the protein does not undergo global conformational changes and that the localized structural rearrangements are also distinct from the mechanisms reported for other cluster A-I SBPs, notably the “spring-hammer” [PsaA (Couñago et al., 2014)], “partial domain slippage” [ZnuA (Chandra et al., 2007)] and the recently reported “trap-door” of AdcA (Luo et al., 2021). The data show that Zn(II)-binding in AdcAII is accompanied by localized structural rearrangements in the C-terminal lobe and stabilization of two loops that close the metal binding site from bulk solvent. Residue His65 appears to transition in and out of the coordination sphere, while His205 drives conformational changes in the C-terminal lobe, and Glu280 remains relatively static. Although the contribution of residue His141 to conformational changes remains unclear, it is unlikely to exhibit movement by virtue of its location deep within the binding pocket. Thus, residues His141 and Glu280 likely comprise the relatively pre-formed metal-binding site, with His65 and His205 playing a more dynamic role in Zn(II) binding. The interaction of His65 with Zn(II) facilitates movement of loop  $\alpha 2\beta 2$  onto the binding site. Interestingly, although loop  $\alpha 2\beta 2$  is mobile in AdcAII, it lacks the extensive mobility observed for the comparable loop in AdcA (Luo et al., 2021). This highlights that loop  $\alpha 2\beta 2$  contributes differently to the Zn(II) recruitment process in the two SBPs, despite their interaction with the same transporter. Conformational changes in the C-terminal lobe are driven by residue His205 in loop  $\alpha 6\beta 5$ ,

which directly pulls  $\beta 5$  into a  $\beta$ -sheet with  $\beta 6$ , causing  $\beta 6$  to tilt down and allowing loop  $\alpha 7\beta 6$  to close over the metal-binding site. Consequently, helices  $\alpha 7$  and  $\alpha 8$  are also pulled towards the metal-binding site. In the absence of Zn(II), the hydrogen bonds between  $\beta 5$  and  $\beta 6$  are largely not formed, and loop  $\alpha 7\beta 6$  is relaxed and moves away from the binding site. Stabilization of these structural elements in the C-terminal lobe may contribute to interaction of AdcAII with AdcB, although further studies will be required to investigate SBP-transporter interaction and the dynamics of Zn(II) release and import. In summary, AdcAII undergoes localized structural rearrangements upon Zn(II) coordination by two of the four coordinating residues, whereby the stabilization of flexible loops and the C-terminal lobe facilitates the transition to a closed conformation.

## DISCUSSION

*S. pneumoniae* survival is dependent on the efficacious acquisition of Zn(II) from the host during infection (Bayle et al., 2011; Plumptre et al., 2014), with prior studies establishing the crucial role of AdcAII in initial infection and invasive disease (Plumptre et al., 2014; Brown et al., 2016). Here, we have shown that AdcAII is highly conserved at the amino acid sequence level in *S. pneumoniae* strains. This suggests that, distinct from other major surface proteins associated with virulence and disease such as PspA (Rapola et al., 2000) and PspC (Georgieva et al., 2018), AdcAII is not influenced by the selective pressures that drive antigenic variation. Whether this is due to poor immunogenicity of AdcAII limiting an antibody-mediated immune response, the antibody-targeted epitopes being shielded in some manner from surveillance, or a slow rate of evolution due to mutations not being tolerated in *adcAII*, remains to be determined. This work highlights that while mutations of the binding site do impact protein function, they do not necessarily compromise bacterial viability and growth in



an *in vitro* context. This raises the question as to whether affinity for Zn(II) is important in absolute terms. The high affinity observed in AdcAII may have arisen as an evolutionary by-product in achieving an optimal conformation transition from the open, metal-free state to the closed, metal-bound closed state of the SBP. Simply put, the necessity of the SBP to be able to efficiently close upon Zn(II)-binding in order to productively interact with AdcCB transporter and thereby facilitate Zn(II) uptake, may have been the dominant selective pressure. The absolute affinity for Zn(II) ions, whether sub-nanomolar or micromolar, the range observed in other Zn(II)-specific SBPs, may not be crucial. Further studies of Zn(II)-specific systems and their relevant niches may provide further insight into this speculation.

The molecular and structural characterization of the AdcAII binding site mutants provides insight into the Zn(II) recruitment mechanism of the protein. Similar to other Zn(II)-specific SBPs, the metal-binding mechanism in AdcAII arises from localized conformational rearrangements within the SBP. The structural rearrangements in the C-terminal lobe of AdcAII have been observed in *E. coli* ZnuA (PDB: 2PS0 [Zn(II)-bound]; 2PS3 [metal-free]), suggesting that  $\beta$ -sheet formation and subsequent rotation of the  $\alpha$ -helices are common features of Zn(II) SBPs (Yatsunyk et al., 2008). Structural studies of ZnuA, as well as *P. denitrificans* AztC (PDB: 5W57 and 5W56), *Candidatus* Liberibacter asiaticus ZnuA2 (PDB: 4UDN and 4UDO) and *S. pneumoniae* AdcA (PDB: 7JJ9 [AdcA] and 7JJ8 [N-terminal AdcA domain]) also show that the N-terminal lobe binding site His residue and the loop in which it resides, His65 and loop  $\alpha 2\beta 2$  in AdcAII, are commonly engaged in structural rearrangements upon Zn(II)-binding (Yatsunyk et al., 2008; Sharma et al., 2015; Neupane et al., 2017; Luo et al., 2021). However, our study reveals that although the Zn(II)-induced conformational changes are relatively subtle, their concerted action is required for high ligand affinity and optimal uptake of Zn(II). Preservation of these structural elements, notably loops  $\alpha 2\beta 2$  and  $\alpha 7\beta 6$  and the associated regions that facilitate their localized rearrangements, may be the underlying basis for the high degree of sequence conservation of *adcAII* across *S. pneumoniae* strains. Unexpectedly, the Zn(II)-binding mechanism of AdcA and AdcAII are subtly different despite both SBPs recruiting the same metal ligand and releasing it to the same transporter, AdcCB. In AdcA, the dynamic mobility of loop  $\alpha 2\beta 2$  has a crucial role in bacterial Zn(II) uptake. By contrast, although AdcAII loop  $\alpha 2\beta 2$  and His65 undergo a conformational transition during Zn(II)-binding, this loop region lacks the flexibility observed in AdcA and is less crucial in Zn(II)-binding and bacterial Zn(II) uptake. Further, loop  $\alpha 7\beta 6$  in the C-terminal lobe appears to be static in AdcA, whereas this region undergoes a conformational transition in AdcAII during Zn(II)-binding. Thus, these data suggest that metal-free AdcAII likely samples a more open conformation than metal-free AdcA.

The increased solvent accessibility and less rigidly defined metal-binding site in AdcAII provides a plausible explanation for the greater promiscuity of cation interaction. Although Zn(II)-bound AdcAII has near-identical coordination geometry to AdcA, the latter protein is restricted to only binding Zn(II),

while AdcAII can interact with a broad range of divalent cations similar to *E. coli* ZnuA (Yatsunyk et al., 2008), *S. pneumoniae* PsaA (Couñago et al., 2014), and *Candidatus* ZnuA2 (Sharma et al., 2015). This has been attributed to the inherent flexibility of the amino acid side chains that comprise the metal-binding site in these SBPs, resulting in an inability to exclude cations other than Zn(II) from interacting and binding. The *in vitro* metal-binding and DSF data suggest that AdcAII is able to interact and potentially transition to a metal-bound, closed conformation with the non-cognate metal ions Co(II) and Cu(II). However, in the nasopharynx, the primary physiological niche colonized by *S. pneumoniae*, AdcAII is unlikely to encounter appreciable levels of these metal ions. Both Co(II) and Cu(II) are relatively low abundance elements in nasopharyngeal tissue, with Co(II) also frequently occurring as a cobalamin chelate in biological systems (Eijkelkamp et al., 2019). Thus, the promiscuity of AdcAII is unlikely to influence asymptomatic colonization of the pathogen. However, it may be a factor during invasive disease, where Cu(II) abundance can increase significantly (Eijkelkamp et al., 2019).

Unexpectedly, affinity for Zn(II), *in vitro* Zn(II)-binding, thermostability of the AdcAII-Zn(II) complex, and impact on bacterial growth were not congruently aligned for the mutant variants. It is notable that AdcAII<sub>H205L</sub> retained *in vitro* Zn(II)-binding and affinity for Zn(II) to the greatest extent but was heavily compromised in the DSF assay and in supporting bacterial growth in Zn(II)-limited medium. By contrast, AdcAII<sub>E280Q</sub> supported wild-type bacterial growth and was the least perturbed variant in the DSF assays but showed reduced *in vitro* Zn(II)-binding and affinity for Zn(II). It is tempting to speculate that the relative degree of conformational impact revealed by the mutant variant crystal structures is the dominant determinant for the observed functional impact. In isolation, this inference provides a plausible explanation for the observed effect on bacterial Zn(II) uptake in the *adcAII* mutant strains. However, while consistent with the data presented herein, this conclusion does not account for the contribution of AdcAII conformational dynamics (in the metal-free and metal-bound states) and interaction of protein-metal complexes with the AdcCB transporter, which remain to be determined. Further, it is important to note that there are energy barriers traversed during the metal-binding process that cannot be addressed by MD simulations using metal-free SBP states generated *via* the *in silico* removal of the Zn(II) ion from a closed, metal-bound structure. This latter issue is an unavoidable technical limitation arising from the absence of a metal-free crystal structure for AdcAII. Despite these caveats, our data suggest that the transition to a closed conformation contributes to efficacious bacterial Zn(II) uptake.

In addition to its metal ion selectivity and mechanistic differences, AdcAII also differs from AdcA in terms of accessory elements used for Zn(II) recruitment. Notably, AdcAII lacks the His-rich loop present in most Zn(II)-specific SBPs, which has recently been shown to aid in sampling bulk solvent for Zn(II) ions in AdcA (Luo et al., 2021) and in other Zn(II)-specific SBPs (Wei et al., 2007; Falconi et al., 2011; Neupane et al., 2017). AdcAII also lacks the C-terminal extension of AdcA that encodes a polypeptide with similarity to the ZinT protein of Gram-negative bacteria. In AdcA, this C-terminal domain also

aids in Zn(II) recruitment (Plumptre et al., 2014; Luo et al., 2021). Despite lacking these structural features, AdcAII has the capacity to interact with four capsule-embedded Pht proteins, PhtABDE, to aid in Zn(II) uptake (Plumptre et al., 2014; Luo et al., 2021). *In vitro* biophysical studies have suggested direct interaction between AdcAII and PhtD, but definitive *in vivo* interaction studies remain to be performed (Loisel et al., 2011; Bersch et al., 2013). Thus, although the mechanistic basis for how AdcAII and the Pht proteins interact remains unclear, these two protein systems cooperatively support efficacious recruitment of Zn(II) in restricted nutritional conditions.

In conclusion, this work presents new insight into the structural and biochemical aspects of AdcAII. This study shows further variation on the mechanistic pathways to recruit Zn(II) ions by a cluster A-I SBP within a common protein architecture. This is particularly notable in *S. pneumoniae*, as despite the differences in Zn(II) recruitment, both AdcA and AdcAII facilitate transport of the bound metal *via* the ABC transporter, AdcCB. This work also suggests that SBP conformation may be more crucial than affinity in terms of Zn(II) acquisition, although *in vivo* experiments remain to be performed. Collectively, these structural and functional insights into AdcAII provide new mechanistic knowledge of the SBP that will be essential for the development of antimicrobial therapeutics targeting the pneumococcal Zn(II) acquisition pathways at the host-pathogen interface.

## DATA AVAILABILITY STATEMENT

The datasets presented in this study can be found in online repositories. The names of the repository/repositories and accession number(s) can be found below: <http://www.wwpdb.org/>, 7LM5; <http://www.wwpdb.org/>, and 7LM6; <http://www.wwpdb.org/>, 7LM7.

## AUTHOR CONTRIBUTIONS

MŽ, ED, BK, and CM contributed to conception and design of the study. MŽ and VP performed the microbiological assays. ZL performed the structural studies. ED performed the molecular

dynamics studies. KG performed the ICP-MS. SN contributed strains, constructs, and supervised MŽ. MŽ wrote the first draft of the manuscript. ZL and ED wrote sections of the manuscript. MŽ and CM revised and integrated the manuscript text. All authors contributed to the article and approved the submitted version.

## FUNDING

This research was undertaken with the assistance of resources and services from the National Computational Infrastructure (NCI), which is supported by the Australian Government and by resources provided by The Pawsey Supercomputing Centre with funding from the Australian Government and the Government of Western Australia. This research was also undertaken using the LIEF HPC-GPGPU Facility hosted at the University of Melbourne. This Facility was established with the assistance of Australian Research Council (ARC) LIEF Grant LE170100200. This work was supported by the National Health and Medical Research Council (NHMRC) grants 1071659 to BK, 1122582 to CM and 1180826 to BK and CM. This work was also supported by the ARC Discovery Project Grant to CM (DP170102102). SN is an NHMRC Early Career Research Fellows (1142695), ED is a UTS Chancellor's Postdoctoral Fellow, BK is an ARC Laureate Fellow (FL180100109), and CM is an ARC Future Fellow (FT170100006).

## ACKNOWLEDGMENTS

We also acknowledge the use of the Australian Synchrotron MX beamlines and the facilities of the Australian Microscopy & Microanalysis Research Facility at the Centre for Microscopy and Microanalysis, The University of Queensland.

## SUPPLEMENTARY MATERIAL

The Supplementary Material for this article can be found online at: <https://www.frontiersin.org/articles/10.3389/fcimb.2021.729981/full#supplementary-material>

## REFERENCES

- Abraham, M., Murtola, T., Schulz, R., Páll, S., Smith, J. C., Jess, B., et al. (2015). GROMACS: High Performance Molecular Simulations Through Multi-Level Parallelism From Laptops to Supercomputers. *SoftwareX* 1-2, 19–25. doi: 10.1016/j.softx.2015.06.001
- Adams, P. D., Afonine, P. V., Bunkoczi, G., Chen, V. B., Davis, I. W., Echols, N., et al. (2010). PHENIX: A Comprehensive Python-Based System for Macromolecular Structure Solution. *Acta Crystallogr. D* 66, 213–221. doi: 10.1107/S0907444909052925
- Afonine, P. V., Grosse-Kunstleve, R. W., Echols, N., Headd, J. J., Moriarty, N. W., Mustyakimov, M., et al. (2012). Towards Automated Crystallographic Structure Refinement With Phenix.Refine. *Acta Crystallogr. D* 68, 352–367. doi: 10.1107/S0907444912001308
- Ammendola, S., Pasquali, P., Pistoia, C., Petrucci, P., Petrarca, P., Rotilio, G., et al. (2007). High-Affinity Zn<sup>2+</sup> Uptake System ZnuABC Is Required for Bacterial Zinc Homeostasis in Intracellular Environments and Contributes to the Virulence of *Salmonella enterica*. *Infect. Immun.* 75, 5867–5876. doi: 10.1128/IAI.00559-07
- Andreini, C., Banci, L., Bertini, I., and Rosato, A. (2006). Zinc Through the Three Domains of Life. *J. Proteome Res.* 5, 3173–3178. doi: 10.1021/pr0603699
- Bayle, L., Chimalapati, S., Schoehn, G., Brown, J., Vernet, T., and Durmort, C. (2011). Zinc Uptake by *Streptococcus pneumoniae* Depends on Both AdcA and AdcAII and Is Essential for Normal Bacterial Morphology and Virulence. *Mol. Microbiol.* 82, 904–916. doi: 10.1111/j.1365-2958.2011.07862.x
- Berendsen, H. J. C., Postma, J. P. M., van Gunsteren, W. F., and Hermans, J. (1981). Interaction Models for Water in Relation to Protein Hydration. *Intermolecular Forces* 14, 331–342. doi: 10.1007/978-94-015-7658-1\_21
- Berendsen, H. J. C., Postma, J. P. M., van Gunsteren, W. F., Dinola, A., and Haak, J. R. (1984). Molecular Dynamics With Coupling to an External Bath. *J. Chem. Phys.* 81, 3684–3690. doi: 10.1063/1.448118
- Bersch, B., Bougault, C., Roux, L., Favier, A., Vernet, T., and Durmort, C. (2013). New Insights Into Histidine Triad Proteins: Solution Structure of a

- Streptococcus pneumoniae* PhtD Domain and Zinc Transfer to AdcAll. *PLoS One* 8, e81168. doi: 10.1371/journal.pone.0081168
- Boylan, J. A., Posey, J. E., and Gherardini, F. C. (2003). *Borrelia* Oxidative Stress Response Regulator, BosR: A Distinctive Zn-Dependent Transcriptional Activator. *Proc. Natl. Acad. Sci. U. S. A.* 100, 11684–11689. doi: 10.1073/pnas.2032956100
- Brown, L. R., Gunnell, S. M., Cassella, A. N., Keller, L. E., Scherkenbach, L. A., Mann, B., et al. (2016). AdcAll of *Streptococcus pneumoniae* Affects Pneumococcal Invasiveness. *PLoS One* 11, e0146785. doi: 10.1371/journal.pone.0146785
- Cerasi, M., Ammendola, S., and Battistoni, A. (2013). Competition for Zinc Binding in the Host-Pathogen Interaction. *Front. Cell. Infect. Microbiol.* 3, 108. doi: 10.3389/fcimb.2013.00108
- Chandra, B. R., Yogavel, M., and Sharma, A. (2007). Structural Analysis of ABC-Family Periplasmic Zinc Binding Protein Provides New Insights Into Mechanism of Ligand Uptake and Release. *J. Mol. Biol.* 367, 970–982. doi: 10.1016/j.jmb.2007.01.041
- Chien, C. C., Huang, C. H., and Lin, Y. W. (2013). Characterization of a Heavy Metal Translocating P-Type ATPase Gene From an Environmental Heavy Metal Resistance *Enterobacter* sp. Isolate. *Biotechnol. Appl. Biochem.* 169, 1837–1846. doi: 10.1007/s12010-012-0047-4
- Couñago, R. M., Ween, M. P., Begg, S. L., Bajaj, M., Zuegg, J., O'Mara, M. L., et al. (2014). Imperfect Coordination Chemistry Facilitates Metal Ion Release in the Psa Permease. *Nat. Chem. Biol.* 10, 35–41. doi: 10.1038/nchembio.1382
- Daura, X., Gademann, K., Jaun, B., Seebach, D., van Gunsteren, W. F., and Mark, A. E. (1999a). Peptide Folding: When Simulation Meets Experiment. *Angewandte Chemie* 38, 236–240. doi: 10.1002/(SICI)1521-3773(19990115)38:1/2<236::AID-ANIE236>3.0.CO;2-M
- Daura, X., van Gunsteren, W. F., and Mark, A. E. (1999b). Folding-Unfolding Thermodynamics of a Beta-Heptapeptide From Equilibrium Simulations. *Proteins* 34, 269–280. doi: 10.1002/(SICI)1097-0134(19990215)34:3<269::AID-PROT1>3.0.CO;2-3
- Davies, M. R., McIntyre, L., Mutreja, A., Lacey, J. A., Lees, J. A., Towers, R. J., et al. (2019). Atlas of Group A Streptococcal Vaccine Candidates Compiled Using Large-Scale Comparative Genomics. *Nat. Genet.* 51, 1035–1043. doi: 10.1038/s41588-019-0417-8
- Desrosiers, D. C., Sun, Y. C., Zaidi, A. A., Eggers, C. H., Cox, D. L., and Radolf, J. D. (2007). The General Transition Metal (Tro) and Zn<sup>2+</sup> (Znu) Transporters in *Treponema pallidum*: Analysis of Metal Specificities and Expression Profiles. *Mol. Microbiol.* 65, 137–152. doi: 10.1111/j.1365-2958.2007.05771.x
- Dintilhac, A., Alloing, G., Granadel, C., and Claverys, J. P. (1997). Competence and Virulence of *Streptococcus pneumoniae*: Adc and PsaA Mutants Exhibit a Requirement for Zn and Mn Resulting From Inactivation of Putative ABC Metal Permeases. *Mol. Microbiol.* 25, 727–739. doi: 10.1046/j.1365-2958.1997.5111879.x
- Eijkelkamp, B. A., Morey, J. R., Neville, S. L., Tan, A., Pederick, V. G., Cole, N., et al. (2019). Dietary Zinc and the Control of *Streptococcus pneumoniae* Infection. *PLoS Pathog.* 15, e1007957. doi: 10.1371/journal.ppat.1007957
- Eijkelkamp, B. A., Morey, J. R., Ween, M. P., Ong, C. L., McEwan, A. G., Paton, J. C., et al. (2014). Extracellular Zinc Competitively Inhibits Manganese Uptake and Compromises Oxidative Stress Management in *Streptococcus pneumoniae*. *PLoS One* 9, e89427. doi: 10.1371/journal.pone.0089427
- Emsley, P., Lohkamp, B., Scott, W. G., and Cowtan, K. (2010). Features and Development of *Coot*. *Acta Crystallogr. D* 66, 486–501. doi: 10.1107/S0907444910007493
- Evans, P. R., and Murshudov, G. N. (2013). How Good are My Data and What is the Resolution? *Acta Crystallogr. D* 69, 1204–1214. doi: 10.1107/S0907444913000061
- Falconi, M., Oteri, F., Di Palma, F., Pandey, S., Battistoni, A., and Desideri, A. (2011). Structural-Dynamical Investigation of the ZnuA Histidine-Rich Loop: Involvement in Zinc Management and Transport. *J. Computer-Aided Mol. Design* 25, 181–194. doi: 10.1007/s10822-010-9409-6
- Georgieva, M., Kagedan, L., Lu, Y. J., Thompson, C. M., and Lipsitch, M. (2018). Antigenic Variation in *Streptococcus pneumoniae* PspC Promotes Immune Escape in the Presence of Variant-Specific Immunity. *mBio* 9 (2), e00264-18. doi: 10.1128/mBio.00264-18
- Gladstone, R. A., Lo, S. W., Lees, J. A., Croucher, N. J., van Tonder, A. J., Corander, J., et al. (2019). International Genomic Definition of Pneumococcal Lineages, to Contextualise Disease, Antibiotic Resistance and Vaccine Impact. *EBioMedicine* 43, 338–346. doi: 10.1016/j.ebiom.2019.04.021
- Grass, G., Franke, S., Taudte, N., Nies, D. H., Kucharski, L. M., Maguire, M. E., et al. (2005). The Metal Permease ZupT From *Escherichia coli* Is a Transporter With a Broad Substrate Spectrum. *J. Bacteriol.* 187, 1604–1611. doi: 10.1128/JB.187.5.1604-1611.2005
- Guex, N., and Peitsch, M. C. (1997). SWISS-MODEL and the Swiss-Pdb Viewer: An Environment for Comparative Protein Modeling. *Electrophoresis* 18, 2714–2723. doi: 10.1002/elps.1150181505
- Handali, M., Neupane, D. P., Roychowdhury, H., and Yukl, E. T. (2015). Transcriptional Regulation, Metal Binding Properties and Structure of Pden1597, an Unusual Zinc Transport Protein From *Paracoccus denitrificans*. *J. Biol. Chem.* 290, 11878–11889. doi: 10.1074/jbc.M115.645853
- Hantke, K. (2005). Bacterial Zinc Uptake and Regulators. *Curr. Opin. Microbiol.* 8, 196–202. doi: 10.1016/j.mib.2005.02.001
- Hennigar, S. R., and McClung, J. P. (2016). Nutritional Immunity: Starving Pathogens of Trace Minerals. *Am. J. Lifestyle Med.* 10, 170–173. doi: 10.1177/1559827616662917
- Henriques-Normark, B., and Normark, S. (2010). Commensal Pathogens, With a Focus on *Streptococcus pneumoniae*, and Interactions With the Human Host. *Exp. Cell Res.* 316, 1408–1414. doi: 10.1016/j.yexcr.2010.03.003
- Humphrey, W., Dalke, A., and Schulten, K. (1996). VMD: Visual Molecular Dynamics. *J. Mol. Graphics Modelling* 14, 33–38, 27–38. doi: 10.1016/0263-7855(96)00018-5
- Kabsch, W. (2010). XDS. *Acta Crystallogr. D* 66, 125–132. doi: 10.1107/S0907444909047337
- Karlinsky, J. E., Maguire, M. E., Becker, L. A., Crouch, M. L., and Fang, F. C. (2010). The Phage Shock Protein PspA Facilitates Divalent Metal Transport and is Required for Virulence of *Salmonella enterica* sv. Typhimurium. *Mol. Microbiol.* 78, 669–685. doi: 10.1111/j.1365-2958.2010.07357.x
- Kearse, M., Moir, R., Wilson, A., Stones-Havas, S., Cheung, M., Sturrock, S., et al. (2012). Geneious Basic: An Integrated and Extendable Desktop Software Platform for the Organization and Analysis of Sequence Data. *Bioinformatics* 28, 1647–1649. doi: 10.1093/bioinformatics/bts199
- Kehl-Fie, T. E., and Skaar, E. P. (2010). Nutritional Immunity Beyond Iron: A Role for Manganese and Zinc. *Curr. Opin. Struct. Biol.* 14, 218–224. doi: 10.1016/j.cbpa.2009.11.008
- Lewinson, O., Lee, A. T., and Rees, D. C. (2009). A P-Type ATPase Importer That Discriminates Between Essential and Toxic Transition Metals. *Proc. Natl. Acad. Sci. U. S. A.* 106, 4677–4682. doi: 10.1073/pnas.0900666106
- Lewis, V. G., Ween, M. P., and McDevitt, C. A. (2012). The Role of ATP-Binding Cassette Transporters in Bacterial Pathogenicity. *Protoplasma* 249, 919–942. doi: 10.1007/s00709-011-0360-8
- Lhospice, S., Gomez, N. O., Ouerdane, L., Brutesco, C., Ghseini, G., Hajjar, C., et al. (2017). *Pseudomonas aeruginosa* Zinc Uptake in Chelating Environment is Primarily Mediated by the Metallophore Pseudopaline. *Sci. Rep.* 7, 17132. doi: 10.1038/s41598-017-16765-9
- Lim, K. H., Jones, C. E., vanden Hoven, R. N., Edwards, J. L., Falsetta, M. L., Apicella, M. A., et al. (2008). Metal Binding Specificity of the MntABC Permease of *Neisseria gonorrhoeae* and its Influence on Bacterial Growth and Interaction With Cervical Epithelial Cells. *Infect. Immun.* 76, 3569–3576. doi: 10.1128/IAI.01725-07
- Loisel, E., Chimalapati, S., Bougault, C., Imbert, A., Gallet, B., Di Guilmi, A. M., et al. (2011). Biochemical Characterization of the Histidine Triad Protein PhtD as a Cell Surface Zinc-Binding Protein of Pneumococcus. *Biochemistry* 50, 3551–3558. doi: 10.1021/bi200012f
- Loisel, E., Jacquamet, L., Serre, L., Bauvois, C., Ferrer, J. L., Vernet, T., et al. (2008). AdcAll, a New Pneumococcal Zn-Binding Protein Homologous With ABC Transporters: Biochemical and Structural Analysis. *J. Mol. Biol.* 381, 594–606. doi: 10.1016/j.jmb.2008.05.068
- Luo, Z., Morey, J. R., Deplazes, E., Motyguillina, A., Tan, A., Ganio, K., et al. (2021). A Trap-Door Mechanism for Zinc Acquisition by *Streptococcus pneumoniae* AdcA. *mBio* 12, e01958–e01920. doi: 10.1128/mBio.01958-20
- Lu, J., Stewart, A. J., Sadler, P. J., Pinheiro, T. J., and Blindauer, C. A. (2008). Albumin as a Zinc Carrier: Properties of its High-Affinity Zinc-Binding Site. *Biochem. Soc. Trans.* 36, 1317–1321. doi: 10.1042/BST0361317
- McDevitt, C. A., Ogunniyi, A. D., Valkov, E., Lawrence, M. C., Kobe, B., McEwan, A. G., et al. (2011). A Molecular Mechanism for Bacterial Susceptibility to Zinc. *PLoS Pathog.* 7, e1002357. doi: 10.1371/journal.ppat.1002357
- McPhillips, T. M., McPhillips, S. E., Chiu, H. J., Cohen, A. E., Deacon, A. M., Ellis, P. J., et al. (2002). Blu-Ice and the Distributed Control System: Software for Data Acquisition and Instrument Control at Macromolecular Crystallography Beamlines. *J. Synchrotron Radiat.* 9, 401–406. doi: 10.1107/S0909049502015170

- Michaud-Agrawal, N., Denning, E. J., Woolf, T. B., and Beckstein, O. (2011). MDAnalysis: A Toolkit for the Analysis of Molecular Dynamics Simulations. *J. Comput. Chem.* 32, 2319–2327. doi: 10.1002/jcc.21787
- Miyamoto, S., and Kollman, P. A. (1992). Settle: An Analytical Version of the SHAKE and RATTLE Algorithm for Rigid Water Models. *J. Comput. Chem.* 13, 952–962. doi: 10.1002/jcc.540130805
- Morey, J. R., and Kehl-Fie, T. E. (2020). Bioinformatic Mapping of Opine-Like Zincophore Biosynthesis in Bacteria. *mSystems* 5 (4), e00554-20. doi: 10.1128/mSystems.00554-20
- Neupane, D. P., Avalos, D., Fullam, S., Roychowdhury, H., and Yukl, E. T. (2017). Mechanisms of Zinc Binding to the Solute-Binding Protein AztC and Transfer From the Metallochaperone AztD. *J. Biol. Chem.* 292, 17496–17505. doi: 10.1074/jbc.M117.804799
- Neville, S. L., Eijkelkamp, B. A., Lothian, A., Paton, J. C., Roberts, B. R., Rosch, J. W., et al. (2020). Cadmium Stress Dictates Central Carbon Flux and Alters Membrane Composition in *Streptococcus pneumoniae*. *Commun. Biol.* 3, 694. doi: 10.1038/s42003-020-01417-y
- Page, A. J., De Silva, N., Hunt, M., Quail, M. A., Parkhill, J., Harris, S. R., et al. (2016). Robust High-Throughput Prokaryote *De Novo* Assembly and Improvement Pipeline for Illumina Data. *Microbial Genomics* 2, e000083. doi: 10.1099/mgen.0.000083
- Pederick, V. G., Eijkelkamp, B. A., Begg, S. L., Ween, M. P., McAllister, L. J., Paton, J. C., et al. (2015). ZnuA and Zinc Homeostasis in *Pseudomonas aeruginosa*. *Sci. Rep.* 5, 13139. doi: 10.1038/srep13139
- Petrarca, P., Ammendola, S., Pasquali, P., and Battistoni, A. (2010). The Zur-Regulated ZinT Protein Is an Auxiliary Component of the High-Affinity ZnuABC Zinc Transporter That Facilitates Metal Recruitment During Severe Zinc Shortage. *J. Bacteriol.* 192, 1553–1564. doi: 10.1128/JB.01310-09
- Plumtre, C. D., Eijkelkamp, B. A., Morey, J. R., Behr, F., Counago, R. M., Ogunniyi, A. D., et al. (2014). AdcA and AdcAII Employ Distinct Zinc Acquisition Mechanisms and Contribute Additively to Zinc Homeostasis in *Streptococcus pneumoniae*. *Mol. Microbiol.* 91, 834–851. doi: 10.1111/mpi.12504
- Rapola, S., Jantti, V., Haikala, R., Syrjanen, R., Carlone, G. M., Sampson, J. S., et al. (2000). Natural Development of Antibodies to Pneumococcal Surface Protein A, Pneumococcal Surface Adhesin A, and Pneumolysin in Relation to Pneumococcal Carriage and Acute Otitis Media. *J. Infect. Dis.* 182, 1146–1152. doi: 10.1086/315822
- Reyes-Caballero, H., Guerra, A. J., Jacobsen, F. E., Kazmierczak, K. M., Cowart, D., Koppolu, U. M., et al. (2010). The Metalloregulatory Zinc Site in *Streptococcus pneumoniae* AdcR, a Zinc-Activated MarR Family Repressor. *J. Mol. Biol.* 403, 197–216. doi: 10.1016/j.jmb.2010.08.030
- Ryckaert, J.-P., Cicotti, G., and Berendsen, H. J. C. (1977). Numerical Integration of the Cartesian Equations of Motion of a System With Constraints: Molecular Dynamics of N-Alkanes. *J. Comput. Phys.* 23, 327–341. doi: 10.1016/0021-9991(77)90098-5
- Sabri, M., Houle, S., and Dozois, C. M. (2009). Roles of the Extraintestinal Pathogenic *Escherichia coli* ZnuACB and ZupT Zinc Transporters During Urinary Tract Infection. *Infect. Immun.* 77, 1155–1164. doi: 10.1128/IAI.01082-08
- Schmid, N., Eichenberger, A. P., Choutko, A., Riniker, S., Winger, M., Mark, A. E., et al. (2011). Definition and Testing of the GROMOS Force-Field Versions 54A7 and 54B7. *Eur. Biophysics J.* 40, 843–856. doi: 10.1007/s00249-011-0700-9
- Sharma, N., Selvakumar, P., Bhose, S., Ghosh, D. K., Kumar, P., and Sharma, A. K. (2015). Crystal Structure of a Periplasmic Solute Binding Protein in Metal-Free, Intermediate and Metal-Bound States From *Candidatus* Liberibacter asiaticus. *J. Struct. Biol.* 189, 184–194. doi: 10.1016/j.jsb.2015.01.012
- Sung, C. K., Li, H., Claverys, J. P., and Morrison, D. A. (2001). An rpsL Cassette, janus, for Gene Replacement Through Negative Selection in *Streptococcus pneumoniae*. *Appl. Environ. Microbiol.* 67, 5190–5196. doi: 10.1128/AEM.67.11.5190-5196.2001
- Terwilliger, T. C., Grosse-Kunstleve, R. W., Afonine, P. V., Moriarty, N. W., Zwart, P. H., Hung, L. W., et al. (2008). Iterative Model Building, Structure Refinement and Density Modification With the PHENIX Autobuild Wizard. *Acta Crystallogr. D* 64, 61–69. doi: 10.1107/S090744490705024X
- Wei, B., Randich, A. M., Bhattacharyya-Pakrasi, M., Pakrasi, H. B., and Smith, T. J. (2007). Possible Regulatory Role for the Histidine-Rich Loop in the Zinc Transport Protein, ZnuA. *Biochemistry* 46, 8734–8743. doi: 10.1021/bi700763w
- Weiser, J. N., Ferreira, D. M., and Paton, J. C. (2018). *Streptococcus pneumoniae*: Transmission, Colonization and Invasion. *Nat. Rev. Microbiol.* 16, 355–367. doi: 10.1038/s41579-018-0001-8
- Yatsunyk, L. A., Easton, J. A., Kim, L. R., Sugarbaker, S. A., Bennett, B., Brece, R. M., et al. (2008). Structure and Metal Binding Properties of ZnuA, a Periplasmic Zinc Transporter From *Escherichia coli*. *J. Biol. Inorganic Chem.* 13, 271–288. doi: 10.1007/s00775-007-0320-0
- Yukl, E. (2017). The Cluster A-I Solute-Binding Proteins. *Encyclopedia Inorganic Bioinorg. Chem.* 1. doi: 10.1002/9781119951438.eibc2512

**Author Disclaimer:** The content of this study is solely the responsibility of the authors and does not necessarily represent the official views of the funding bodies.

**Conflict of Interest:** The authors declare that the research was conducted in the absence of any commercial or financial relationships that could be construed as a potential conflict of interest.

**Publisher's Note:** All claims expressed in this article are solely those of the authors and do not necessarily represent those of their affiliated organizations, or those of the publisher, the editors and the reviewers. Any product that may be evaluated in this article, or claim that may be made by its manufacturer, is not guaranteed or endorsed by the publisher.

Copyright © 2021 Župan, Luo, Ganio, Pederick, Neville, Deplazes, Kobe and McDevitt. This is an open-access article distributed under the terms of the Creative Commons Attribution License (CC BY). The use, distribution or reproduction in other forums is permitted, provided the original author(s) and the copyright owner(s) are credited and that the original publication in this journal is cited, in accordance with accepted academic practice. No use, distribution or reproduction is permitted which does not comply with these terms.